Desalination and Water Treatment
www.deswater.com
doi: 10.5004/dwt.2019.23431

142 (2019) 37–48
February

Embedded high-hydrophobic CNMs prepared by CVD technique with PVDF-co-HFP membrane for application in water desalination by DCMD

Mustafa Mohammed Aljumaily[a], Mohammed Abdulhakim Alsaadi[a,b,*], N. Awanis Hashim[c,*], Qusay F. Alsalhy[d,*], Rasel Das[a], Farouq S. Mjalli[e]

[a]*Nanotechnology & Catalysis Research Centre (NANOCAT), University of Malaya, IPS Building, Kuala Lumpur 50603, Malaysia; email: mustafa.kh1989@gmail.com (M.M. Aljumaily), Tel. +60163630693; emails: mdsd68j@gmail.com (M.A. Alsaadi), raselgeneticist@gmail.com (R. Das)*
[b]*National Chair of Materials Science and Metallurgy, University of Nizwa, Nizwa, Sultanate of Oman*
[c]*Department of Chemical Engineering, University of Malaya, Kuala Lumpur 50603, Malaysia, Tel. +60196888638; email: awanis@um.edu.my*
[d]*Membrane Technology Research Unit, Chemical Engineering Department, University of Technology, Alsinaa Street No. 52, B.O. 35010, Baghdad, Iraq; email: qusay_alsalhy@yahoo.com, 80001@uotechnology.edu.iq*
[e]*Department of Petroleum and Chemical Engineering, Sultan Qaboos University, P.O. Box 33, Muscat 123, Oman; email: farouqsm@yahoo.com*

Received 8 May 2018; Accepted 7 November 2018

ABSTRACT

In this work, conditions for fabricating high-hydrophobic carbon nanomaterials (CNMs) by chemical vapor deposition technique on nickel-doped powder activated carbon such as reaction temperature, reaction time, and H_2:CH_4 gas ratio were optimized to achieve the optimum contact angle (CA). The results showed that the optimal reaction temperature, H_2:CH_4 gas ratio, and reaction time for the highest CA of 145° were 950°C, 1:1, and 20 min, respectively. The CNM with a CA of 145° was embedded with poly(vinylidene fluoride-co-hexafluoropropylene) (PVDF-co-HFP) membrane to improve its hydrophobicity and, in turn, its seawater desalination performance by direct contact membrane distillation (DCMD). Various CNM contents (i.e., 1.0, 3.0 and 5.0 wt.%) were embedded with 22:78 (wt.%) of PVDF-co-HFP/N-Methyl-2-pyrrolidone solution to prepare flat-sheet membranes via phase inversion. CNM content plays an important role in the membrane preparation and thus affected the DCMD performance. Particularly interesting was the membrane prepared from dope mixture with the 5 wt.% CNMs, which resulted in an increase in CA from 83° to 133°, and porosity from 45.3% to 96.94%, along with a decrease in the membrane thickness from 210 to 165 μm. However, CNM embedding into the casting mixture also affected the membrane's mechanical properties. Finally, DCMD permeation was enhanced from 10 to 16 L/hm^2 by embedding 5 wt.% of CNMs at the feed temperature of 45°C with salt rejection >99.9%.

Keywords: Chemical vapour deposition; Carbon nanomaterials; Hydrophobicity; PVDF-co-HFP; Direct contact membrane distillation; Desalination

1. Introduction

Seawater had become a major alternative to freshwater in order to address the increasing demand and compensate for freshwater supply shortages [1]. Growing concern over freshwater shortage has led to membrane distillation (MD) as an alternative technique for seawater treatment [2]. MD is a thermally-driven process based on the vapor partial pressure across a hydrophobic membrane [3]. Saline water is in direct contact with the hydrophobic membrane surface in all MD configurations. The hydrophobic membrane acts as a barrier between the hot seawater feed and the cold

* Corresponding authors.

freshwater permeate, a process referred to as direct contact membrane distillation (DCMD) [4,5]. The membrane hydrophobicity prevents liquids from mixing, while water vapor travels within the micropores due to the water vapor partial pressure, which acts as the driving force [6].

To be effective, the membrane should have appropriate structure in terms of pore size and porosity, as well as physicochemical properties suitable for the MD applications [7]. The poly(vinylidene fluoride-co-hexafluoropropylene) (PVDF-co-HFP) is a polymer that has attracted attention as a potential membrane for MD applications [8]. Compared with other polymers, PVDF-co-HFP has lower crystallinity because HFP is an integral part of the PVDF, which develops the amorphous phase content that leads to better hydrophobic chains [9]. The hydrophobic characteristics of the membrane surface are highly dependent on its chemical composition and geometric properties. Water wettability through the contact angle (CA) measurement is used as an indicator of the membrane hydrophobic properties [10]. Surfaces with <90° are considered hydrophilic, while those having CA > 90° are hydrophobic [10–12]. Exceptionally CA > 150° are classified as super-hydrophobic [13,14].

With the advent of nanotechnology, various nanomaterials (NMs) have attracted tremendous scientific attention, as they are believed to contribute to greater membrane hydrophobicity. Decreasing NM dimensions increases the membrane surface area, as well as alters the 2D and 3D crystallinity. This, in turn, affects surface wettability as well as mechanical, thermal, and chemical properties, which may prompt development of more sustainable, efficient, reliable, and affordable novel membrane technologies. Examples of such techniques are membrane filtration [15,16] and MD [17,18].

In order to attain a hydrophobic carbon nanomaterials (CNMs) that can be used for scaling-up membrane processes, chemical vapor deposition (CVD) is presently used, as it satisfies the requirements of high yield and enhanced performance [19]. The CVD method is based on a hydrocarbon cracking process, as a part of which free carbon atoms are deposited on a metal catalyst at high temperatures to form carbon nanostructures with different physicochemical properties. Different substrates have been used in CVD on which hydrophobic CNMs are typically grown. However, these substrates might cause CNM aggregation and often contain impurities. Therefore, cleaning and washing processes are required to eliminate these impurities, as their presence adversely affects the surface of CNM and dramatically reduces the CA [20]. In the present study, powder activated carbon (PAC) served as the substrate for synthesizing CNM that is suitable for membrane fabrication. PAC was selected because it is an available and economical substrate for CNM growth [21] and, unlike other substrates, PAC does not need to be chemically or physically removed from the functional bulk material [22]. The PAC-CNM hybrid exhibited PAC properties, as well as those unique to CNMs.

Furthermore, the CVD process was optimized by changing the production process parameters to obtain the highest CA for CNMs grown on PAC. This was achieved using a Design of Experiment/Response Surface (DoE/RS) model to achieve the optimum CA. According to the findings yielded by our previous studies, CNMs could be used in the development of water-repellent industrial-grade technologies [14]. In this work, the produced CNM grown on PAC was utilized to fabricate a PVDF-co-HFP/CNM membrane that was tested in a DCMD setup that was designed specifically for the present study to examine its water desalination effectiveness.

2. Materials and methods

2.1. Chemicals and reagents

Nickel (II) nitrate hexahydrate, PAC, acetone, methane (CH_4), hydrogen (H_2), and nitrogen (N_2) were purchased from Sigma-Aldrich, Malaysia. All chemicals were of analytical grade. The membrane material, PVDF-co-HFP, was also purchased from Sigma-Aldrich, as was N-Methyl-2-pyrrolidone (NMP, >99.5%), which was used as a solvent.

2.2. Carbon nanomaterials synthesis and membrane fabrication

2.2.1. Catalyst impregnation

1 wt. % of nickel (II)-acetone solution was prepared in 5 ml of acetone grade, >95% purity and mixed with 2 g of PAC using sonication at 50°C and 40 kHz until the acetone evaporated. The Ni-doped PAC was dried in an oven at 75°C overnight. The dried sample was ground thoroughly, and the Ni-doped PAC powder was stored in a desiccator until required.

2.2.2. Carbon nanomaterials growth using chemical vapor deposition

The CNM-PAC superstructure was synthesized by placing Ni-doped PAC onto a ceramic boat within the CVD reaction tube described by Aljumaily et al. [14]. The temperature was programed to perform calcination at 350°C for 2 h under inert atmosphere (N_2, 200 ml/min), followed by reduction at 450°C under (H_2, 150 ml/min) in the 650°C–950°C range, as shown in Fig. 1. CH_4 was mixed with H_2 at a 1:4 ratio, and the mixture was passed through the reaction tube for 20–60 min. After the CNM growth, the reactor was cooled down using N_2 flow (200 ml/min) and the CNM was collected from the ceramic boat.

2.2.3. CA measurement

The CA between the CNM and water was calculated by placing a drop of their mixture (4 µl) onto glass microscope slides (76 × 26 × 1.2 mm) covered with a double-sided adhesive tape. A KRUSS Goniometer (DSA100) was used for all CA measurements. Each measurement was performed in triplicate and the average value was adopted.

2.2.4. Experimental design and CA optimization

To reduce the number of experimental runs, a DoE software (central composite design (CCD), Version 7) was used. Three CNM growth conditions were considered, namely, temperature, gas ratio, and contact time. The optimization criteria were identified, as the aim was to maximize CA by minimizing reaction time and temperature. Prior to calculating the optimum solution, a statistical regression model was developed through the DoE. Analysis of variance (ANOVA)

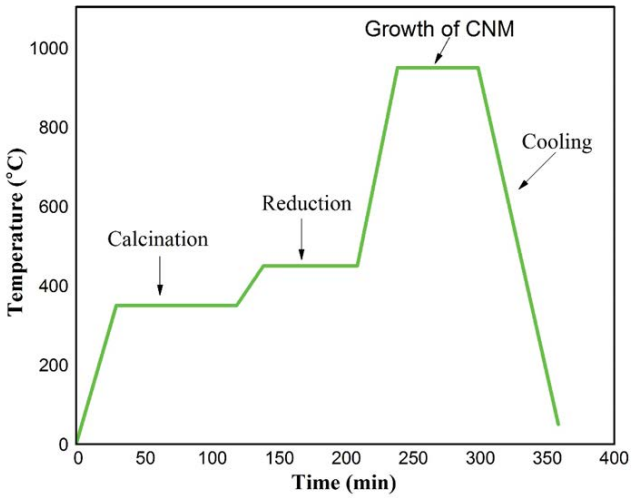

Fig. 1. Temperature profile for the CNMs synthesis using CVD reactor.

was used to determine the significance of the model and the interaction of various parameters.

2.2.5. Preparation of membranes

Blank PVDF-co-HFP/NMP membranes were synthesized by the phase inversion method, following the preparation methods described elsewhere [23,24]. About 22:78 (wt.%/wt.%) polymer to solvent ratio was used. Mixture was mixed overnight using a magnetic stirrer at 400 rpm to assure homogeneity. Various CNM concentrations (1.0, 3.0, and 5.0 wt.%) were added to the mixture according to the PVDF-co-HFP/CNMs weight ratios, namely, 22:0.0, 21:1, 19:3, and 17:5. Next, adequate CNM dispersion was carried out using an ultrasound bath for about 30 min, which was sufficient to obtain a well-dispersed CNM mixture within the polymeric solution. The composite matrix solution was prepared by using casting knife of 250 μm gap into a thin film on a clean glass plate fixed onto the casting machine at room temperature and was exposed to air for 30–60 s. The thin film, together with the glass plate, was subsequently immersed into distilled water until a wet film floated up to the water surface. The membrane was rinsed again with fresh distilled water for 24 h to completely remove any solvent residues. The membranes were subsequently left at room temperature to dry before further use.

2.3. Membrane characterizations

The functional groups that resulted from the mixing of CNMs in the membrane matrix were studied using attenuated total reflection-Fourier transform infrared spectroscopy. The spectra were recorded by a NICOLET 510P spectrometer. The data of composite membrane structure were recorded in the region 4,000–500 cm^{-1}.

CNM surface morphologies and topologies were examined using transmission electron microscopy (TEM; Hitachi-HT7700, 120 kV, Japan). Scanning electron microscope (SEM; XL30 FEG, FEI Company) was used to image the cross-section and surface morphologies of the composite membranes. The dried composite membrane samples were broken in liquid nitrogen before being sputtered with a thin layer of platinum using SPI-module sputter coater.

Membrane porosity ε_m (%) can be defined as the ratio of pore volume to the total membrane volume. The porosity of the membranes was determined according to a gravimetric method based on density measurements compared with the fabricated membrane [25] using Eq. (1):

$$\varepsilon_m(\%) = \left(1 - \frac{\rho_{cm}}{\rho_{control}}\right) \times 100 \quad (1)$$

where ρ_{cm} and $\rho_{control}$ are, respectively, the composite membrane and the PVDF-co-HFP density. The PVDF-co-HFP density of 1.78 g cm^{-3} was adopted, as per the Sigma-Aldrich report.

The atomic force microscope (AFM) 3D images were obtained over different areas, whereby the probe was moved up and down over the surface of each composite membrane sample (of 10 μm × 10 μm size), using Nanoscope III in tapping mode. AFM was used to scan the composite membrane surface with the colloidal probe, whereby topography data and phase signals were obtained simultaneously. The composite membrane surfaces were characterized in terms of the mean roughness and pore size distribution. The same scanning area (10 μm × 10 μm) was utilized to evaluate the pore sizes and the adopted value was based on the average of at least 25 measurements for the composite membrane.

The saltwater sample was prepared by dissolving 35 g of NaCl in 1 l of double-distilled water, as this concentration mimicked raw sea/ocean water. The feed and permeate concentrations were determined by using conductivity and total dissolved solids meter (Extech, Malaysia). The salt rejection, R (%), was calculated using Eq. (2):

$$R(\%) = \left[1 - \left(\frac{C_{pc}}{C_{fc}}\right)\right] \times 100 \quad (2)$$

where C_{pc} and C_{fc} are the permeate and the feed concentrations, respectively.

The composite membranes were subjected to the tensile strength test, performed at room temperature using an Instron 5940 tensile test machine. All samples were clamped at both ends, securing them to the machine, and were pulled at the elongation velocity of 30 mm/min with an initial gauge length of 20 mm, to produce tension. Five samples were measured for each composite membrane and the average was adopted as the final result. Breaking tensile stress, tensile strain, and Young's modulus were obtained.

2.4. Direct contact membrane distillation process

For the DCMD performance test, the membranes were placed inside a testing cell. The DCMD unit consists of two spaces, designated for deionized water and seawater, respectively, which are separated by a double steel stile holding the CNMs composite membrane, as shown in Fig. 2. The composite membrane contact area had a disc shape of 10.4 mm diameter. Two peristaltic pumps were used to control

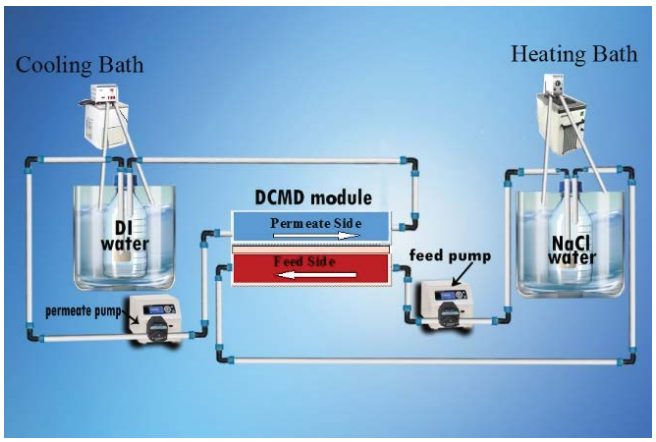

Fig. 2. Schematic representation of the experimental DCMD setup used in this study.

streams at both feed and permeate side, which were pumped in recirculation mode through heat and cool stream exchangers, respectively. The system was operated for 60 min with the feed flow rate of 22 ml/min and the permeate side stream flow rate of 12 ml/min [26]. The temperature on both sides of the DCMD unit was continuously monitored by two thermocouples and was maintained at 45°C (feed side) and 20°C (permeate side). Electrical conductivity of the feed and permeate side, as well as water level transferred to the permeate side, were monitored over time.

3. Results and discussion

3.1. Model establishment and analysis

CNMs were deposited on PAC/Ni from CH_4 precursor in the CVD reactor. The aim of this process was to obtain the highest possible CA. The CNM growth parameters, namely, temperature, gas ratio, and reaction time were optimized to achieve high-hydrophobic CNMs (as quantified by CA measurements). DoE was used to design the experiments with a minimum number of experimental runs, and the CAs were measured, as summarized in Table 1. The effects of reaction temperature, gas ratio, and reaction time on CH_4 decomposition were studied using the response surface methodology. The data pertaining to 14 runs performed as a part of this analysis were subjected to ANOVA to study the effects of process parameters on CA. The coefficient of determination R-squared (R^2) of the mean (0.7993) and 2FI (0.9225) models showed close correlation. However, the 2FI model was more significant, as its probability, Prob > F, value was 0.0438 < 0.05. The 2FI model was thus chosen for subsequent CA analyses due to the higher R^2 (0.9225).

3.2. Statistical analysis and modeling

The data obtained by performing the aforementioned 14 runs are shown in Table 1. The experimental data were fitted to obtain an empirical-statistical model for CA using Eq. (3).

$$CA = 102.85 + 28.22A + 1.83B - 3.07C - 0.26AB + 2.24AC + 2.09BC \quad (3)$$

Table 1
Experimental design matrix and the value of responses based on experiment run

Run	Temperature (°C)	Time (min)	Gas ratio (%)	CA (°)
1	850.00	40.00	2.50	93
2	950.00	20.00	4.00	135
3	750.00	60.00	4.00	75
4	850.00	20.00	2.50	87
5	1,000.00	20.00	1.00	140.3
6	750.00	20.00	4.00	74
7	750.00	60.00	1.00	79
8	950.00	60.00	4.00	140
9	750.00	40.00	2.50	83
10	950.00	20.00	1.00	145
11	850.00	40.00	4.00	80
12	950.00	60.00	1.00	130
13	850.00	60.00	2.50	110
14	750.00	20.00	1.00	80

where A, B, and C represent the reaction temperature, time, and gas ratio, respectively.

A comparison between the experimental results and the model values of predicted from CA, which is indicated by a high R^2 and Eq. (3), is depicted in Fig. 3(a). Fig. 3(b) shows the validation based on fresh experiment data. ANOVA indicators for the CA responses are displayed in Table 2. As evidenced from the ANOVA test results, the reaction temperature (A) was significant, as its >F value was less than 0.05 [24]. Hence, from statistical results and keeping in mind (A) gained the highest multiplier, it can be concluded that temperature had higher impact on CA compared with the remaining parameters. Additionally, an F value of 9.22 implies that the CA model is significant and stable. Moreover, the effect of reaction time and gas ratio, as well as the factor interactions, exist in the model but exert only a minor effect on CA. The interactions between the CNM synthesis parameters and their effect on CA are graphically illustrated by the CCD curves based on the empirical model, as shown in Fig. 4. In Fig. 4(a), depicting the effect of reaction temperature and reaction time on CA, respectively, it can be seen that CA increases with an increase in temperature. Thus, higher temperature should be used to achieve a greater CA. In particular, a significant increase in CA occurred as the reaction temperature increased from 650°C to 950°C, as shown in Fig. 4(a) and (b). These observations confirm that CNM synthesis should be performed at higher temperatures, countering the findings reported by other authors, who considered the yield, rather than CA, as the process response [14,27].

Using a high temperature could accelerate the deposition of graphitic carbon scoots around the Ni-doped PAC, [28] thus contributing to the increase in CNM hydrophobicity. As can be seen from Fig. 3(c), neither reaction time nor gas ratio have a positive effect on CA. In the graph, a steady increase in CA with increasing reaction time for the gas ratio of 4.0 can be noted. However, increasing the gas ratio further decreases the resulting CA. The highest CA was obtained at a gas ratio of 1.0°C and 950°C. This indicates that the gas ratio does not

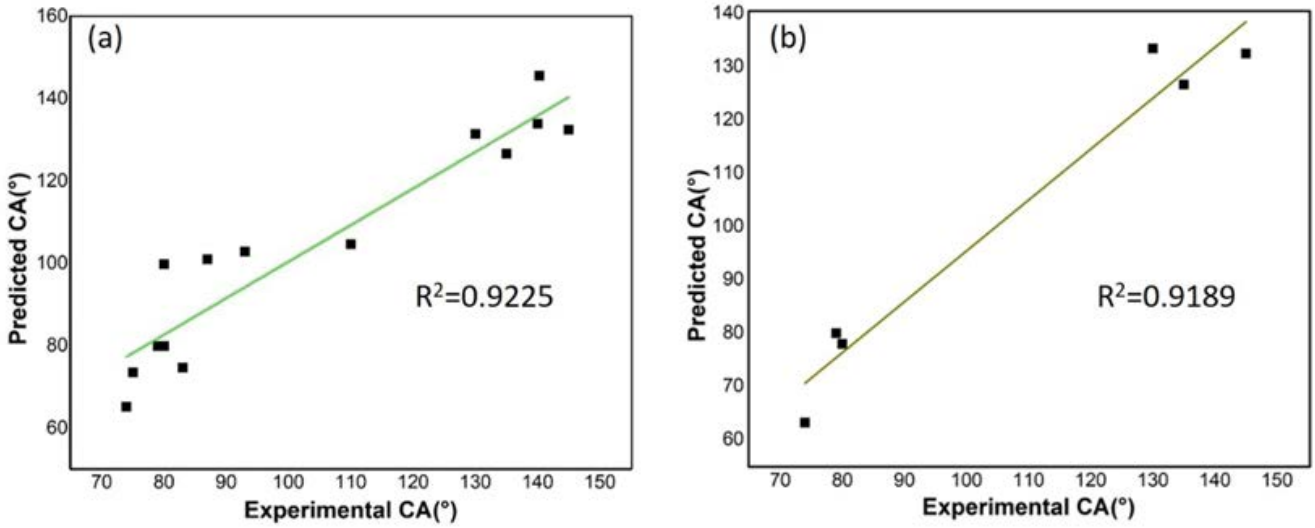

Fig. 3. Parity plot of experimental and predicted values of CA (a) and validation (b).

Table 2
Analysis of variance for CA response surface modified model

Source	Sum of square	DF	Mean square	*F*	Prob. > *F*
A	8,109.35	1	8,109.35	48.91	0.0002
B	34.85	1	34.85	0.21	0.6605
C	89.09	1	89.09	0.54	0.4873
AB	0.64	1	0.64	0.00386	0.9522
AC	45.60	1	45.60	0.28	0.6161
BC	37.09	1	37.09	0.22	0.6506
Model	9,174.56	6	1,529.09	9.22	0.0049

influence the carbon growth nucleation when PAC is used as a support for the Ni catalyst at high temperature and reaction time.

3.2. Optimization study of carbon nanomaterials growth for optimum CA

The CNM synthesis parameters and CA responses were optimized using a CCD methodology, to obtain high-hydrophobic CNMs. All synthesis parameters and responses corresponding to the maximum limits of the synthesis experimental ranges must satisfy the criteria of significant module to determine the optimum conditions. Several combinations were predicted by the DoE to high optimum CA. The optimum synthesis conditions for the highest CA were a reaction temperature of 950°C, a gas ratio of 1.0, and a reaction time of 20 min, which resulted in a CA of 145°, as shown in Table 3. The experiments were performed at the predicted parameter conditions to verify the calculated CA of CNMs. The data show that the predicted CA was in good agreement with the experimental values, with a mean error of 2.21%. The CA of the PAC/Ni and optimized CNM were studied, as shown in Fig. 5(a) and (b), respectively. The PAC/Ni has much lower hydrophobicity (80°) as compared with the optimized CNM (145°) due to the rough surface of the CNMs.

3.3. Membrane characterization

3.3.1. Fourier transform infrared spectroscopy analysis

The functional groups of the composite membranes and PVDF-co-HFP were analyzed by Fourier transform infrared spectroscopy. As can be seen in Fig. 6, a slight predominance of a crystalline phase is observed in the PVDF-co-HFP membrane, as indicated by the presence of transmission peaks at 528, 614, 760, 795, 840, 876, and 973 cm^{-1}. However, 974, 1,070, 1,180, 1,280 and 1,400 cm^{-1} are also observed and are ascribed to the polymer/solvent NMP interactions [8]. It is important to mention here that the spectra revealed the formation of different types of functional groups between residual NMP and PVDF-HFP during the membrane preparation. A peak at 1,660 cm^{-1} related to PVDF-co-HFP/CNMs can be clearly distinguished from the spectrum, which is due to C=O stretching vibrations. The spectrum of CNMs showed different range of functional groups. The dominant peaks at 1,442, 1,445, and 1,552 cm^{-1} were appeared due to stretching vibrations rings and peaks at wave numbers 1,660 cm^{-1} was associated with C=O. In general, CNMs are contaminated on the metal catalysts with amorphous carbon during the synthesis by CVD process of producing CNMs which typically oxidized by air to produce a few functional groups. These findings indicate that the CNM was successfully grafted to the PVDF-co-HFP material.

3.3.2. Scanning electron microscope, porosity and thickness analyses

SEM was used to examine the changes in the composite membrane morphology due to the addition of CNMs. Fig. 7 provides the SEM images for the top surface (a–c) and cross-sections (a–c) of the nanocomposite membranes. A finger-like structure was observed in the cross-section images of the membranes prepared from pure PVDF-co-HFP, whereas the addition of 1 wt.% CNMs changes the cross-section, whereby two layers emerge one finger-like structure near the top surface and a sponge-like structure near the bottom

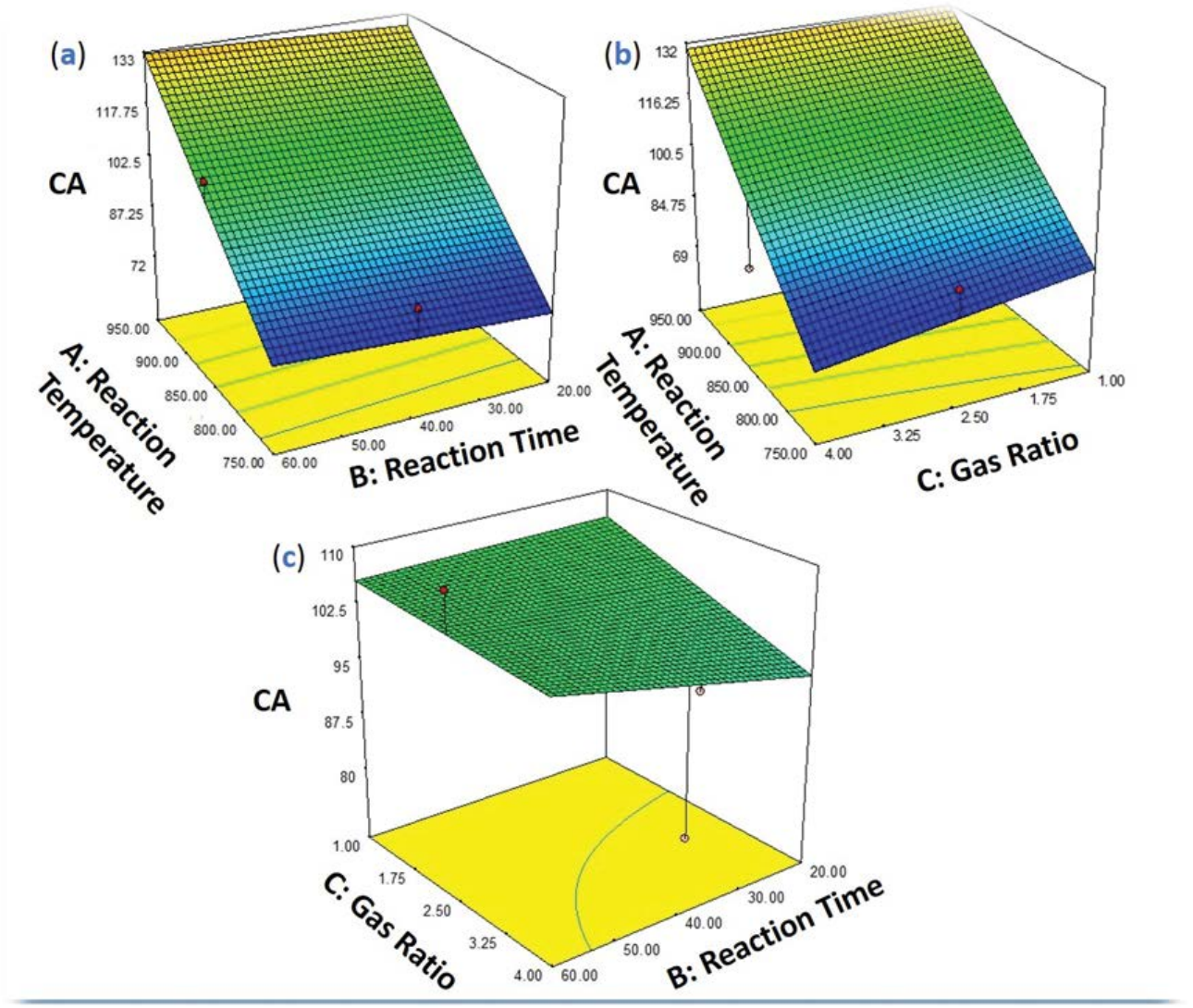

Fig. 4. Response surface plots for the effects of different process parameters on CA. (a) Effect of reaction temperature and reaction time at the optimum fixed gas ratio of 2:1; (b) effect of reaction temperature and gas ratio at the optimum fixed reaction time of 40 min; and (c) effect of gas ratio and reaction time at the optimum fixed reaction temperature of 850°C.

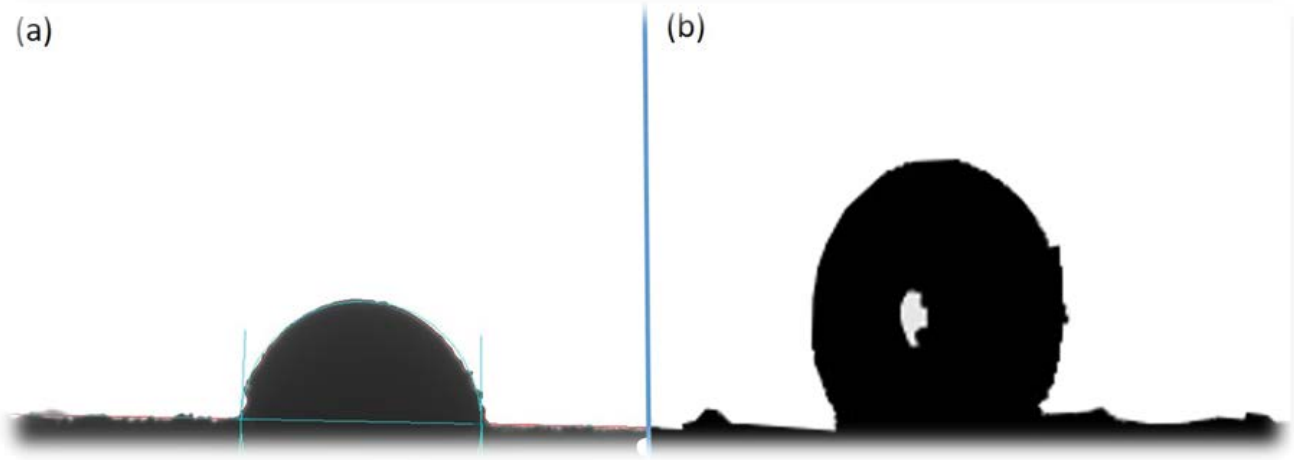

Fig. 5. (a) Contact angle of PAC and (b) CA of CNM.

Table 3
Mechanical performance of PVDF-co-HFP and PVDF-co-HFP/CNMs membranes

Mechanical properties	Tensile strength (MPa)	Elongation at break (%)	Young's modulus (MPa)
PVDF-co-HFP	2.89	186.9	63.55
PVDF-co-HFP/1 wt.% CNMs	2.20	76.7	34.87
PVDF-co-HFP/3 wt.% CNMs	3.10	133.1	52.45
PVDF-co-HFP/5 wt.% CNMs	4.19	283.7	67.98

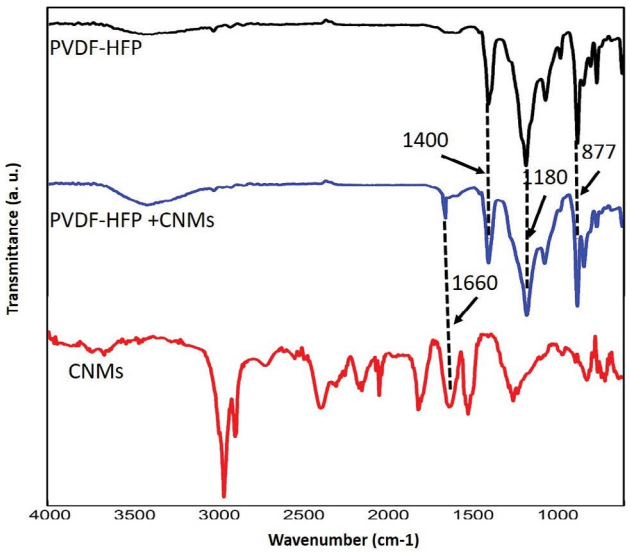

Fig. 6. FT-IR spectra of neat PVDF-co-HFP and composite membranes.

surface, as shown in Fig. 7(a). Further increases in CNM content, for example, to 3 and 5 wt.%, lead to a thinner finger-like structure near the top surface, while the width of the sponge layer near the bottom surface increases, as shown in the cross-section micrographs presented in Fig. 7(b) and (c). When the top surface structure was examined more closely, it was observed that, as the CNM content increased from 1 to 3 wt.%, the pore sizes on the surface increased. Further increases to the CNM content (up to 5 wt.%) resulted in a decrease in the pore size on the top surface, as shown in Fig. 7(a–c). The TEM image shown in Fig. 7(d) reveals the CNMs with a 30–50 nm diameter, which was the optimum size, as determined by the DoE. The membrane structure changes were attributed to a delay in the exchange process between NMP and water through the membrane as a result of CNMs being embedded in the polymer solution [29]. It is important to note that the presence of CNMs in the casting solution is a hindrance for water penetration into the casting solution through the membrane, which was the main reason for the emergence of the sponge layer at the bottom of the membrane cross-section (delay water-NMP demixing process). It is well known that the exchange rate velocity between the solvent and non-solvent (water) has a main factor affecting the structure of the membrane, for example, delay exchange rate results to form membrane with porous structure.

Fig. 8 shows the effect of CNM loading on the porosity and thickness of the fabricated membranes. As CNM loading increased from 1 to 3 wt.%, membrane porosity increased from 61.92% to 68.88%. However, further increases in the CNM loading up to 5 wt.% resulted in a severe porosity increase (up to 96.94%). Therefore, it can be concluded that CNM loading exerts significant effects on the membrane porosity. The porosity increase in the PVDF-co-HFP/CNMs composite membranes is closely linked to the prevalence and interactions of CNMs embedded within the polymer solution, which hinder the NMP/water exchange through the membrane, resulting in a formation of a porous structure.

Regarding the effects of loading the casting solution with CNMs on the composite membrane thickness, it can be observed from Fig. 8 that the thickness of the flat sheet membrane decreased from 210 to 170 μm as the CNM loading increased from 1 to 3 wt.%. However, a further increase to 5 wt.% results in a reduction of the membrane thickness to 165 μm. This effect on membrane thickness was due to the decrement in polymer concentration in the casting solution, which was the main reason for the observed reduction in the membrane thickness.

3.3.3. Atomic force microscope

The 3D AFM images of the top surface of the composite membranes prepared by adding different amounts of highly hydrophobic CNMs loaded to the membrane matrix are shown in Fig. 9. It can be seen that the nodular structure is formed in the top skin of PVDF-co-HFP/CNMs membranes, with interconnected cavity channels between the agglomerated nodules on the top membrane surface. The nodule size increased as the CNM loading in the polymer solution increased from 1 and 3 wt.%, whereas it decreased when 5 wt.% CNM loading was used, as shown in Fig. 9. The change in the rate of diffusion between NMP (solvent) and water (non-solvent) through the membrane was the main cause for the formation of structural nodules on the membrane surface.

It is obvious that the membrane roughness is measured by the vertical distance between nodule peaks and valleys, and there is a direct relation between membrane roughness and its performance. Therefore, the PVDF-co-HFP/CNMs membrane roughness was obtained from the AFM measurements, as shown in Fig. 9. It can be seen that the membrane roughness increases as the CNM loading increases from 1 to 3 wt.%, while addition of 5 wt.% CNM results in a decrease in membrane roughness, which is still greater than that of a membrane free from CNMs. This phenomenon is due to the delay in the exchange rate between solvent and non-solvent

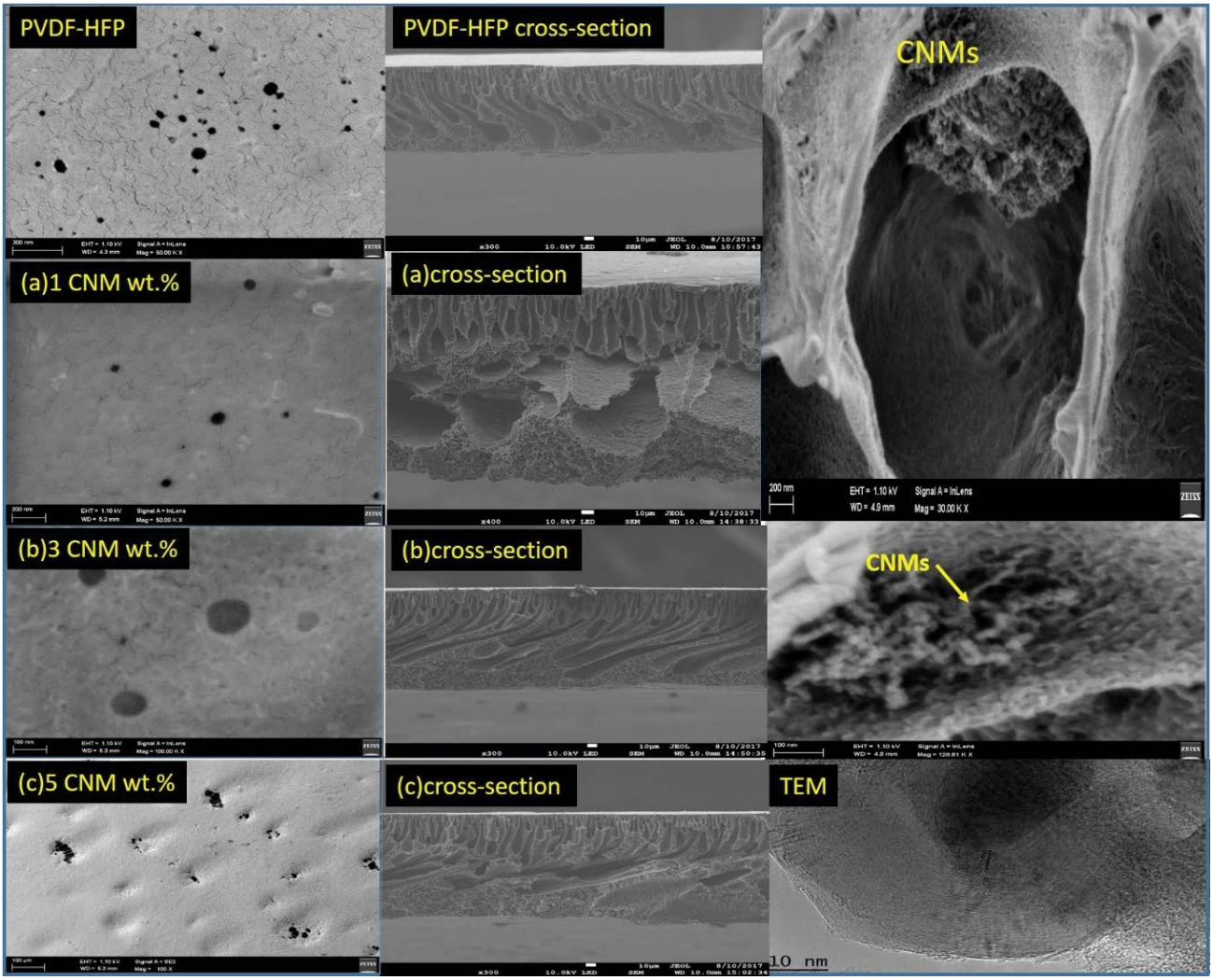

Fig. 7. FE-SEM and TEM micrographs of the cross-sectional area of the composite membranes.

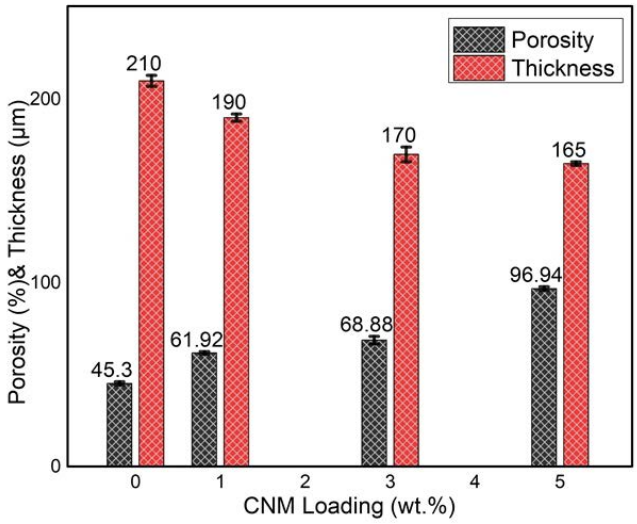

Fig. 8. Effect of CNMs loading in casting solution on porosity and thickness of the composites membrane.

during the membrane formation. On the other hand, the membrane roughness reduction following the addition of 5 wt.% CNM should be closely linked to the formation of some agglomeration and entanglement of CNMs, resulting in non-homogenous distribution, which in turn decreases membrane roughness. The AFM results revealed that CNM loading affects the surface roughness. High roughness is desirable in MD, since it is one of the factors contributing to the membrane flux. The composite membranes were characterized in terms of the average surface roughness (Rave) and pore size distribution. The scan area of 10 μm × 10 μm (in *X* and *Y* direction) was used while the *Z*-axis was set to 1.0 μm recorded by Gwyddion software. As shown in Fig. 10, there are three different regions (lines *A*, *B*, and *C* in Fig. 10) to describe the variant of height of the membrane and pore diameter.

3.3.4. Contact angle of the nanocomposite membrane

CA is one of the important membrane properties, considered as indicators of the ability of water to penetrate through

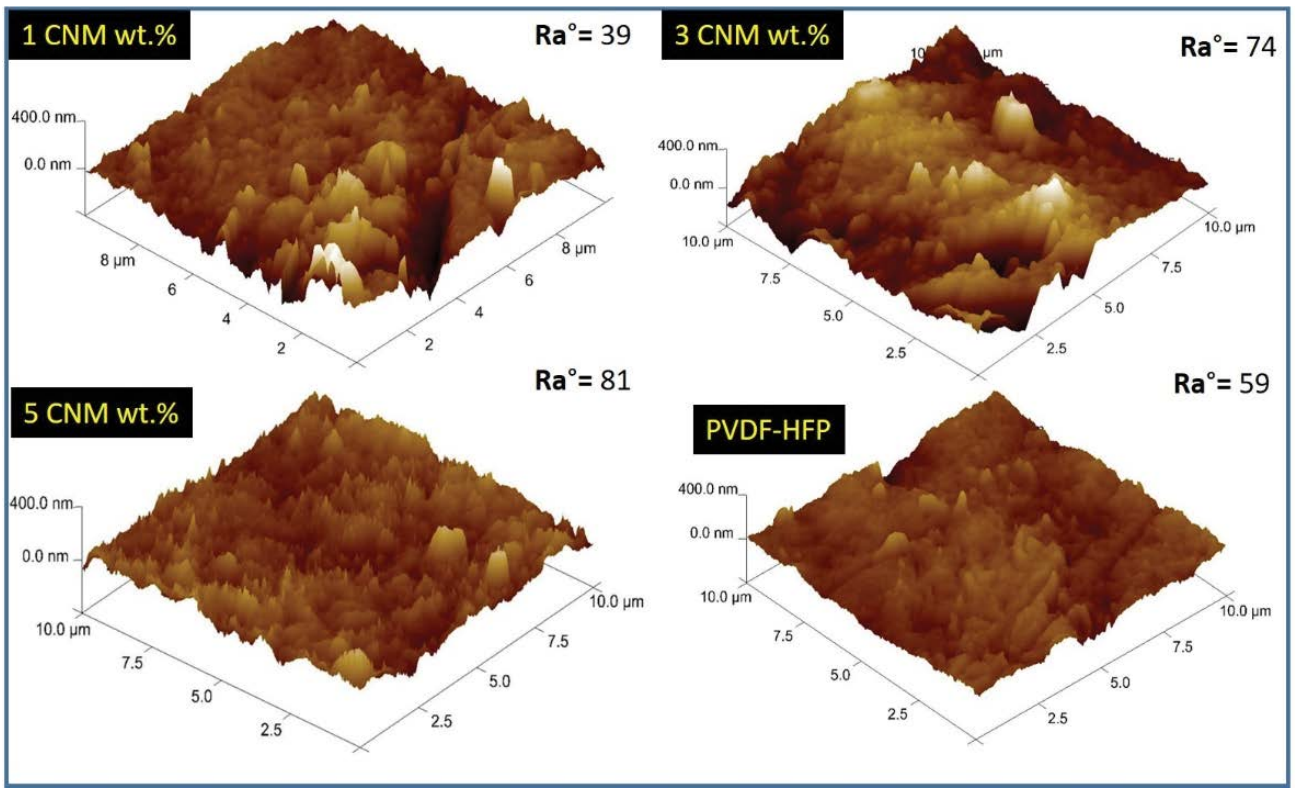

Fig. 9. 3D AFM images of the membrane prepared from various CNMs loading.

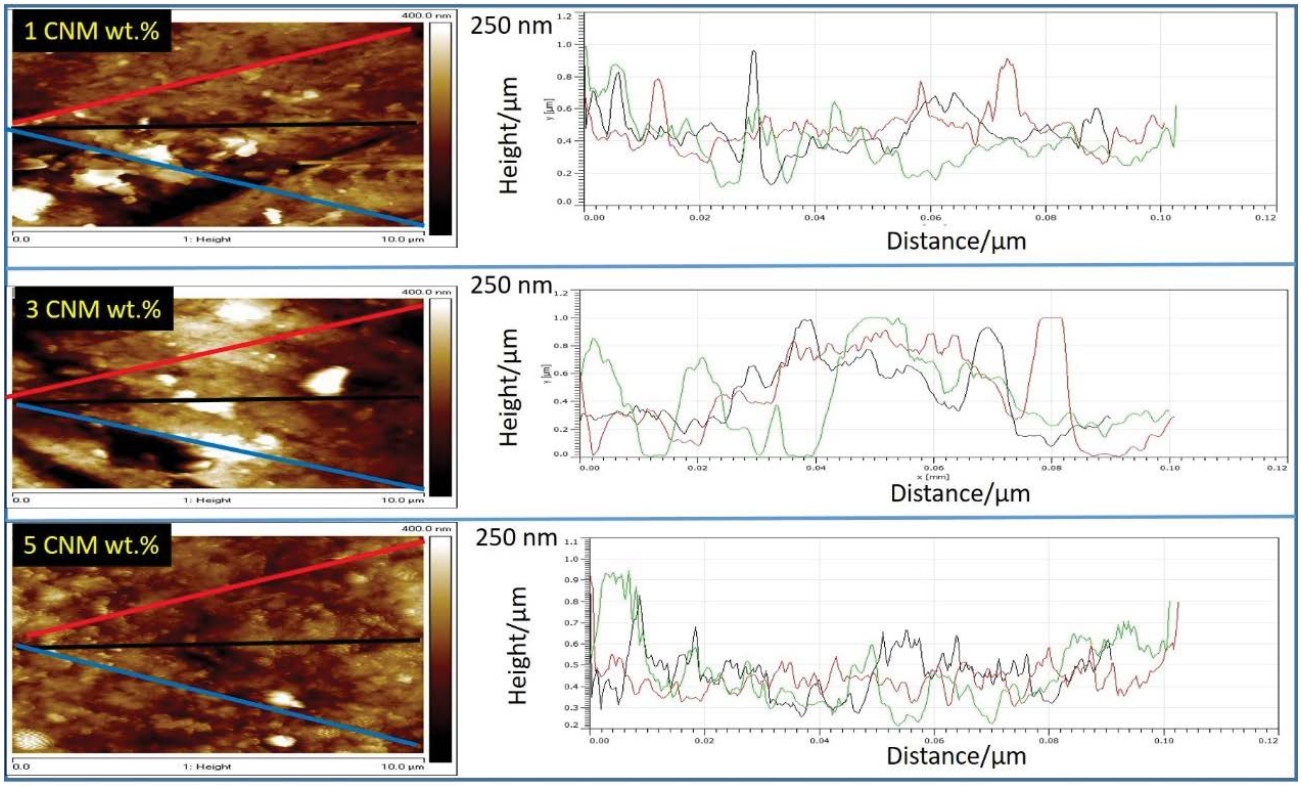

Fig. 10. Effect of CNMs loading on the surface roughness of the membranes.

the membrane wall. In MD processes, the membrane should be hydrophobic in order to prohibit water penetration through its wall, while permitting water vapor diffusion into the membrane body. Therefore, in order to improve membrane hydrophobicity and enhance its performance, CNMs with highly hydrophobic character prepared by the method described above were added to the polymer casting solution with various loadings (i.e., 1, 3, and 5 wt.%). Fig. 11 presents the CAs of the membranes prepared from various CNM loadings in the casting solution. It can be seen that the CA of PVDF-co-HFP/CNMs is improved from 83° to 87° with the increase in the CNM loading to 1 wt.%. A further increase to 3 and 5 wt.% results in a significant increase in the CA to 125° and 133°, respectively. The CA of the membrane prepared from PVDF-co-HFP/CNMs increases due to the significant CNM distribution across the membrane surface. This phenomenon was explained by Madaeni et al. who reported that embedding multiwall carbon nanotubes in the pores of the microfiltration PVDF membrane resulted in the formation of micro- and/or nano-roughness on the external surface of the PDMS-coated layer, thus increasing the membrane roughness [30]. This phenomenon results in air bubbles being trapped in the roughened surface and increases the CA. Consequently, a membrane with hydrophobic properties is formed.

3.3.5. Mechanical stability analysis

To maximize the advantage of adding CNMs as an effective reinforcement for high membrane matrix strength, the CNMs must be well dispersed to improve the interfacial interaction between CNMs and polymer. In order to compare the control (PVDF-co-HFP) membrane to the composite membrane in terms of mechanical properties, asymmetric microporous membranes with 1, 3, and 5 wt.% CNM were tested for stress–strain characteristics. Table 3 shows the mechanical properties of the membrane prepared from PVDF-co-HFP and PVDF-co-HFP/CNMs. When a tensile speed of 140 mm/min was applied to the porous membrane at 20°C, tensile strengths of membranes prepared using 1, 3, and 5 wt.% CNM as additive were 2.209, 3.10, and 4.19 MPa, respectively. In contrast, the tensile strength of PVDF-co-HFP was 2.89 MPa. From these results, it can be conclude that the lack of adhesion between the agglomerated bunches of CNMs and polymer matrix was the main reason for the reduction of tensile strength of the membrane embedded with 1 wt.% of CNMs compare with that prepared from neat PVDF-co-HFP. Farther increase in CNMs amount resulted in forming kind of networking with less separating spaces occupied by the polymer matrix. A more evident difference was obtained for the mechanical properties of various nanocomposite membranes. For example, the elongation percentage at breakage for PVDF-co-HFP/CNMs membrane prepared from 5 wt.% CNM was 283.7%, while that of pure PVDF-co-HFP was 186.9%. Moreover, the elongations at breakage for membranes prepared from 1 and 3 wt.% CNM were lower than that for PVDF-co-HFP, as shown in Table 3. For the Young's modulus, similar behavior was observed where the membrane prepared using 5 wt.% CNM outperformed that prepared from pure PVDF-co-HFP, as well as membranes prepared using 1 and 3 wt.% CNM, as shown in Table 3. These experimental values indicate that some mechanical properties of a membrane with CNMs are superior to the composite membrane, which is one benefit for potential composite membrane materials. The MD process is usually conducted at normal atmospheric pressure; thus, it is estimated that composite membrane pores will not be affected. A good dispersion of CNMs appears to be achieved at 5 wt.%, despite higher CNM loading.

Mechanical properties are always related to the CNM embedding in membranes and the composite membrane crystallinity [8]. Membrane rigidity is increased with CNM loading. In addition, a greater elongation was observed at breakage, accompanied by a decrease in the Young's modulus, which was the highest for the sample prepared with the highest CNM loading. This finding is attributed to the well-embedded CNMs with the polymer phase, which could confer better CNM stability than that of the pure PVDF-co-HFP. The formation of sponge layer on the bottom membrane surface also contributed to the improved mechanical properties, as seen in Fig. 7. According to the published data, the mechanical properties of polymer membranes are mostly enhanced by the addition of a greater percentage of NMs due to the "cross-linking effects" that can mitigate the stress of the membrane load.

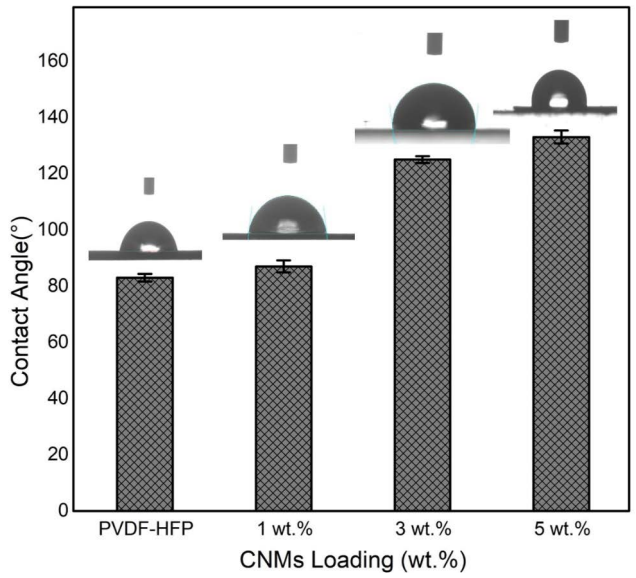

Fig. 11. CA of the (a) PAC/Ni and (b) optimized CNM.

3.3.6. Direct contact membrane distillation performance

The performance of 1, 3, and 5 wt.% nanocomposite membranes was tested in a DCMD setup system, as shown in Fig. 12. CNMs were used to improve the performance of composite membranes in terms of distillation by producing high permeation flux. The permeation flux of the PVDF-co-HFP/CNMs composite membrane increased as the CNM loading increased. The average salt rejection of all membranes remained >99.9% throughout the duration of the experiment. These results show that modification of PVDF-co-HFP by CNM particles can improve the membrane performance for DCMD, as the permeation flux was increased from

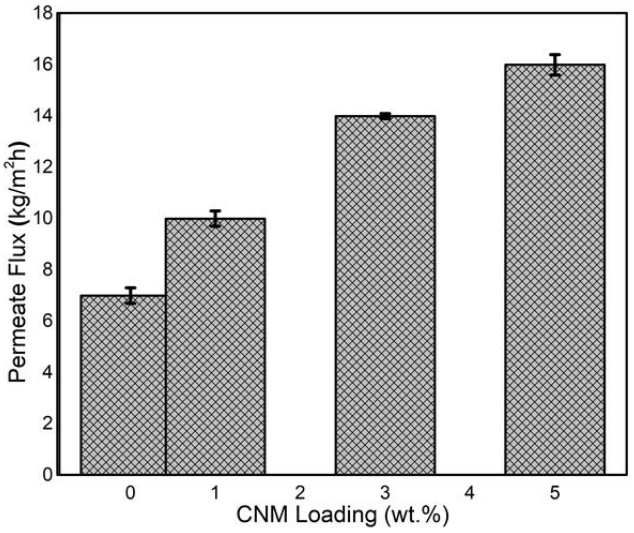

Fig. 12. Effect of CNMs loading on permeate flux at temperature of 45°C.

10 for pure PVDF-co-HFP membrane to 16 L/m²/h for the membrane with 5 wt.% CNM [8,25,29]. This phenomenon is attributed to the increase in membrane porosity and CA, along with decreasing of membrane thickness, as a result of increasing CNM loading, as shown in Figs. 9 and 11, respectively. From the results obtained in this study, it can be concluded that CNMs offer promising opportunities when incorporated into the PVDF-co-HFP solution. In addition to the improvement in CA and porosity by embedding CNMs, the CNMs resulted in high membrane flux capacity and surface area, which may favor the interaction of vapor molecules with CNMs, allowing them to move from the feed side to the permeate side by a surface/intra-particle diffusion process, as reported elsewhere [31].

In comparison with previous work [8], where the membrane was prepared from a mixture comprising of 12 wt.% PVDF-co-HFP and isopropanol solution as a coagulation bath, it can be noticed that, at lower feed temperature of 45°C in this study, similar permeation flux of 16 L/h/m² was obtained to that when 60°C was used in the previous work. This result is due to the higher porosity, lower thickness, and higher CA of the PVDF-co-HFP membrane prepared by using the method described in this work.

4. Conclusions

In this study, statistical experimental analysis findings showed the existence of interaction among the different parameters affecting CNM growth on PAC by CVD. The membrane CA measurements were taken as responses and a significant regression model was obtained, which was used for a successful process parameter optimization. Based on the results obtained experimentally, it was concluded that the temperature plays an important role and that gas ratio and reaction time were significant factors in determining the membrane CA. The process parameter optimization indicated that the best operating conditions were a reaction temperature of 950°C, a gas ratio of 1, and a reaction time of 20 min, which gave the highest CA of 145°. In addition, from the results reported here, it is evident that a PVDF-co-HFP solution with various amounts of CNMs yielded substantial improvements in the morphological structure and hydrophobic character of the membrane, whereby the CA increased from 83° to 133° at 5 wt.% CNMs loading. The composite membrane exhibited a very high salt rejection of >99.9% in most cases, with enhanced permeate flux from 10 to 16 L/m²/h at the feed temperature of 45°C as CNMs loading increases. Furthermore, the composite membrane attained improved mechanical properties as compared with the control polymer-based membrane.

Acknowledgment

The authors would like to acknowledge the National Chair of Materials Sciences and Metallurgy, University of Nizwa, Oman, and the University of Malaya RP044D-17AET for funding this research.

References

[1] Z. Chen, Water Shortages, Urban Water Reuse Handbook, CRC Press, 2016, p. 1.
[2] E. Mathioulakis, V. Belessiotis, E. Delyannis, Desalination by using alternative energy: review and state-of-the-art, Desalination, 203 (2007) 346–365.
[3] Q.F. Alsalhy, S.S. Ibrahim, S.R. Khaleel, Performance of vacuum poly(propylene) membrane distillation (VMD) for saline water desalination, Chem. Eng. Process., 120 (2017) 68–80.
[4] L.F. Dumée, K. Sears, J. Schütz, N. Finn, C. Huynh, S. Hawkins, M. Duke, S. Gray, Characterization and evaluation of carbon nanotube Bucky-Paper membranes for direct contact membrane distillation, J. Membr. Sci., 351 (2010) 36–43.
[5] K.Y. Wang, S.W. Foo, T.-S. Chung, Mixed matrix PVDF hollow fiber membranes with nanoscale pores for desalination through direct contact membrane distillation, Ind. Eng. Chem. Res., 48 (2009) 4474–4483.
[6] A. Alkhudhiri, N. Darwish, N. Hilal, Membrane distillation: a comprehensive review, Desalination, 287 (2012) 2–18.
[7] J. Yin, B. Deng, Polymer-matrix nanocomposite membranes for water treatment, J. Membr. Sci., 479 (2015) 256–275.
[8] S. Fadhil, T. Marino, H.F. Makki, Q.F. Alsalhy, S. Blefari, F. Macedonio, E. Di Nicolò, L. Giorno, E. Drioli, A. Figoli, Novel PVDF-HFP flat sheet membranes prepared by triethyl phosphate (TEP) solvent for direct contact membrane distillation, Chem. Eng. Process., 102 (2016) 16–26.
[9] A.M. Stephan, D. Teeters, Characterization of PVdF-HFP polymer membranes prepared by phase inversion techniques I. Morphology and charge–discharge studies, Electrochim. Acta, 48 (2003) 2143–2148.
[10] F. De Nicola, P. Castrucci, M. Scarselli, F. Nanni, I. Cacciotti, M. De Crescenzi, Super-hydrophobic multi-walled carbon nanotube coatings for stainless steel, Nanotechnology, 26 (2015) 145701.
[11] L.H. Li, Y. Chen, Superhydrophobic properties of nonaligned boron nitride nanotube films, Langmuir, 26 (2010) 5135–5140.
[12] S.Q. He, J.Q. Wei, H.F. Wang, D.S. Sun, Z.H. Yao, C.S. Fu, R.Q. Xu, Y. Jia, H.W. Zhu, K.L. Wang, D.H. Wu, Stable superhydrophobic surface of hierarchical carbon nanotubes on Si micropillar arrays, Nanoscale Res. Lett., 8 (2013) 412.
[13] M. Ma, R.M. Hill, Superhydrophobic surfaces, Curr. Opin. Colloid Interface Sci., 11 (2006) 193–202.
[14] M.M. Aljumaily, M.A. Alsaadi, R. Das, S.B.A. Hamid, N.A. Hashim, M.K. AlOmar, H.M. Alayan, M. Novikov, Q.F. Alsalhy, M.A. Hashim, Optimization of the synthesis of superhydrophobic carbon nanomaterials by chemical vapor deposition, Sci. Rep., 8 (2018) 2778.

[15] R. Das, M.E. Ali, S.B.A. Hamid, S. Ramakrishna, Z.Z. Chowdhury, Carbon nanotube membranes for water purification: a bright future in water desalination, Desalination, 336 (2014) 97–109.
[16] R. Das, S.B.A. Hamid, M.E. Ali, A.F. Ismail, M. Annuar, S. Ramakrishna, Multifunctional carbon nanotubes in water treatment: the present, past and future, Desalination, 354 (2014) 160–179.
[17] P.S. Goh, A.F. Ismail, B.C. Ng, Carbon nanotubes for desalination: performance evaluation and current hurdles, Desalination, 308 (2013) 2–14.
[18] T. Humplik, J. Lee, S. O'hern, B. Fellman, M. Baig, S. Hassan, M. Atieh, F. Rahman, T. Laoui, R. Karnik, Nanostructured materials for water desalination, Nanotechnology, 22 (2011) 292001.
[19] V. Shanov, W. Cho, R. Malik, N. Alvarez, M. Haase, B. Ruff, N. Kienzle, T. Ochmann, D. Mast, M. Schulz, CVD growth, characterization and applications of carbon nanostructured materials, Surf. Coat. Technol., 230 (2013) 77–86.
[20] J. Tittmann-Otto, S. Hermann, J. Kalbacova, M. Hartmann, M. Toader, R. Rodriguez, S. Schulz, D. Zahn, T. Gessner, Effect of cleaning procedures on the electrical properties of carbon nanotube transistors—a statistical study, J. Appl. Phys., 119 (2016) 124509.
[21] A. Mamun, Y. Ahmed, S.A. Muyibi, M. Al-Khatib, A.T. Jameel, M.A. AlSaadi, Synthesis of carbon nanofibers on impregnated powdered activated carbon as cheap substrate, Arabian J. Chem., 9 (2016) 532–536.
[22] J. Ward, B. Wei, P. Ajayan, Substrate effects on the growth of carbon nanotubes by thermal decomposition of methane, Chem. Phys. Lett., 376 (2003) 717–725.
[23] M.K. AlOmar, M.A. Alsaadi, M.M. Aljumaily, S. Akib, T.M. Jassam, M.A. Hashim, N, N-Diethylethanolammonium chloride-based DES-functionalized carbon nanotubes for arsenic removal from aqueous solution, Desalin. Water Treat., 74 (2017) 163–173.
[24] S.-P. Chai, K.-Y. Lee, S. Ichikawa, A.R. Mohamed, Synthesis of carbon nanotubes by methane decomposition over Co–Mo/Al_2O_3: process study and optimization using response surface methodology, Appl. Catal., A, 396 (2011) 52–58.
[25] Q.F. Alsalhy, K.T. Rashid, S.S. Ibrahim, A.H. Ghanim, B. Van der Bruggen, P. Luis, M. Zablouk, Poly (vinylidene fluoride-co-hexafluoropropylene)(PVDF-co-HFP) hollow fiber membranes prepared from PVDF-co-HFP/PEG-600Mw/DMAC solution for membrane distillation, J. Appl. Polym. Sci., 129 (2013) 3304–3313.
[26] T.L. Silva, S. Morales-Torres, J.L. Figueiredo, A.M. Silva, Multi-walled carbon nanotube/PVDF blended membranes with sponge- and finger-like pores for direct contact membrane distillation, Desalination, 357 (2015) 233–245.
[27] H.M. Alayan, M.A. Alsaadi, A. Abo-Hamad, M.K. AlOmar, M.M. Aljumaily, R. Das, M.A. Hashim, Hybridizing carbon nanomaterial with powder activated carbon for an efficient removal of Bisphenol A from water: the optimum growth and adsorption conditions, Desalin. Water Treat., 95 (2017) 128–143.
[28] C. Masarapu, H.F. Zeng, K.H. Hung, B. Wei, Effect of temperature on the capacitance of carbon nanotube supercapacitors, ACS Nano, 3 (2009) 2199–2206.
[29] M. Khayet, C. Cojocaru, M.C. García-Payo, Experimental design and optimization of asymmetric flat-sheet membranes prepared for direct contact membrane distillation, J. Membr. Sci., 351 (2010) 234–245.
[30] S. Madaeni, S. Zinadini, V. Vatanpour, Preparation of superhydrophobic nanofiltration membrane by embedding multiwalled carbon nanotube and polydimethylsiloxane in pores of microfiltration membrane, Sep. Purif. Technol., 111 (2013) 98–107.
[31] S. Bonyadi, T.S. Chung, Flux enhancement in membrane distillation by fabrication of dual layer hydrophilic–hydrophobic hollow fiber membranes, J. Membr. Sci., 306 (2007) 134–146.